UNIVERSITY OF OXFORD

Dynamo on the OMEGA laser and kinetic problems of proton radiography

Archie Bott, Alex Rigby, Tom White, Petros Tzeferacos, Don Lamb, Gianluca Gregori, Alex Schekochihin (and many others…)

2th August 2016

Overview

1. Background/motivation - why achieving dynamo in the laboratory matters

2. Small-scale turbulent dynamo on the OMEGA laser facility
   - Set-up and diagnostics
   - Simulation and plasma characterisation
   - Results – near equipartition of magnetic and kinetic energy

3. Proton radiography of stochastic magnetic fields
   - Kinetic theory of imaging beam
   - Extracting magnetic field statistics from flux images
   - Particle diffusion due to small-scale fields

Background

- Basic question: how did ICM come to be universally magnetised?
  - Typical seed mechanisms inadequate

- Explanation: *small-scale turbulent kinematic dynamo*

- MHD dynamo (mostly) understood theoretically
  - Stretching of field lines at resistive scale

$$\frac{\partial \mathbf{B}}{\partial t} = \nabla \times (\mathbf{u} \times \mathbf{B}) + \eta \nabla^2 \mathbf{B}$$

  - Process well-demonstrated in simulations – need $\mathrm{Rm} \geq 200$

- Understanding of plasma dynamo less developed – but lots of recent progress!

- Turbulent dynamo mechanism never seen in the laboratory due to insufficient Rm
  - Laboratory experiments allow for confirmation of process in more complicated physical situations

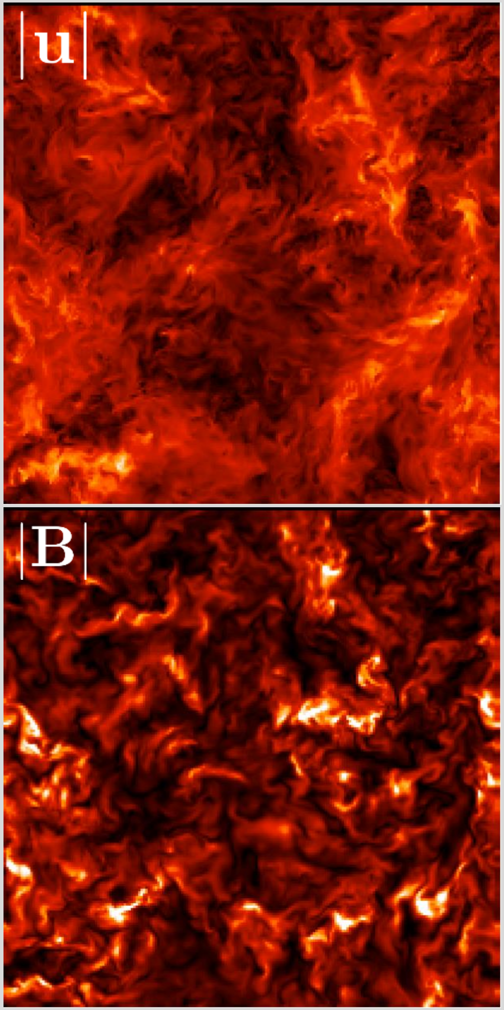

[3] *Simulated small-scale dynamo: Top: velocity; Bottom: magnetic field strength*

OMEGA laser facility

- Located at Laboratory for Laser Energetics (LLE), Rochester, US – built 1995
- 60 beams lines, 40 kJ maximum laser energy (highest energy/pulse until NIF)

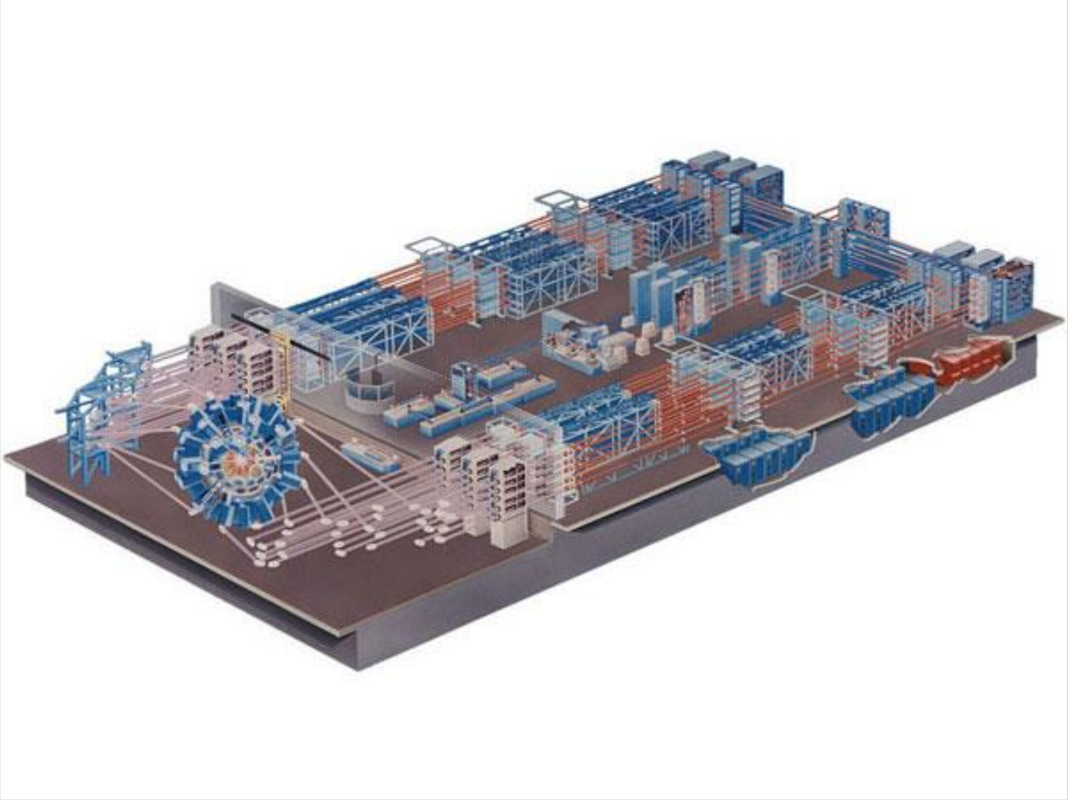

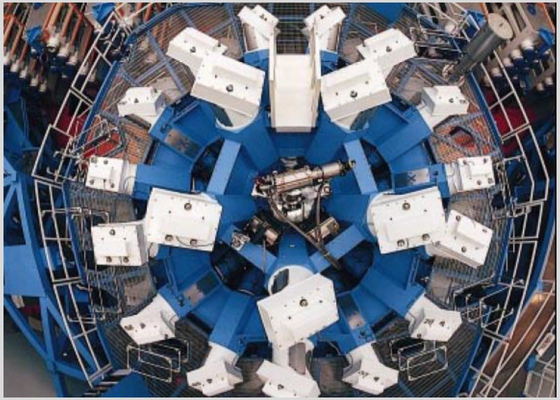

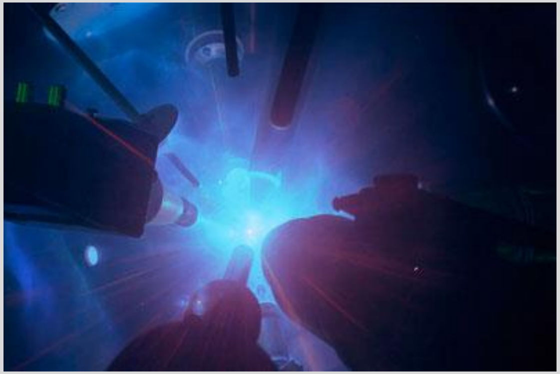

Source: http://www.lle.rochester.edu/omega_facility/omega/

Experimental set-up

- Turbulent region created by colliding unstable laser-driven plasma jets
- Two pulse shapes
  - 5 ns drive gives higher flow velocities (so greater Rm)
- Diagnostics
  - Thomson scattering
  - X-ray framing camera
  - Proton radiography
  - Polarimetry

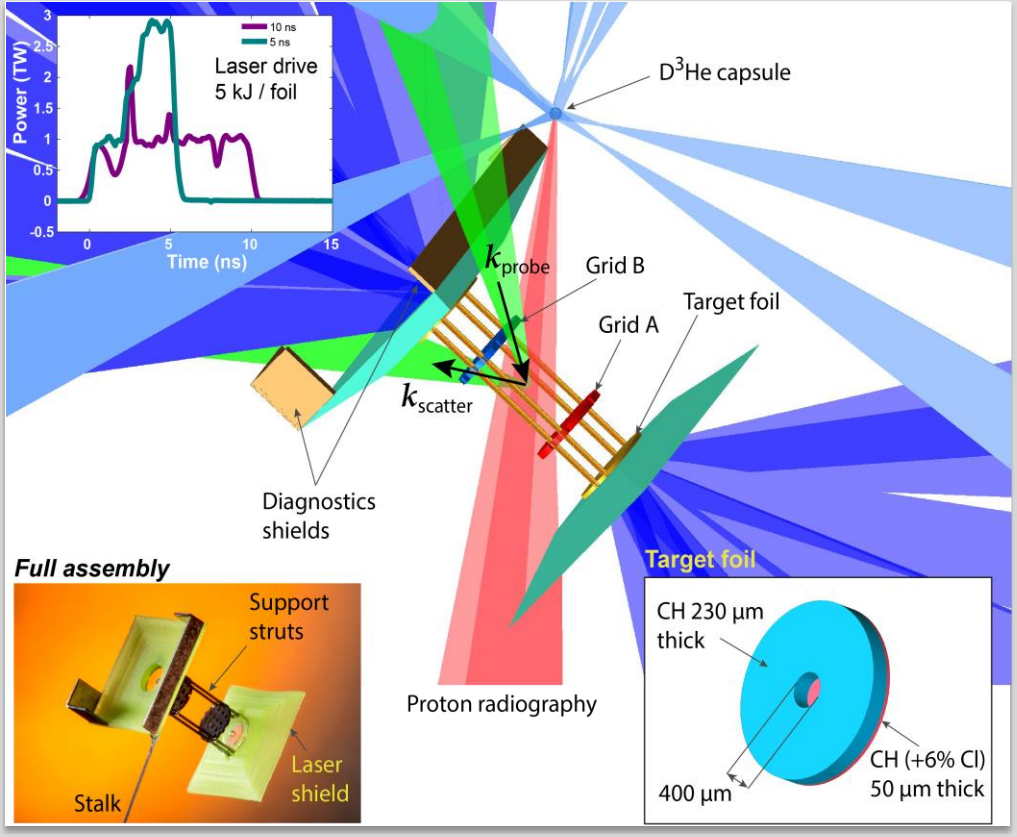

Schematic of experimental set-up, featuring pulse shape (top left), foil design (bottom right) and partial diagnostic layout, along with image of actual target (bottom left)

Thomson scattering

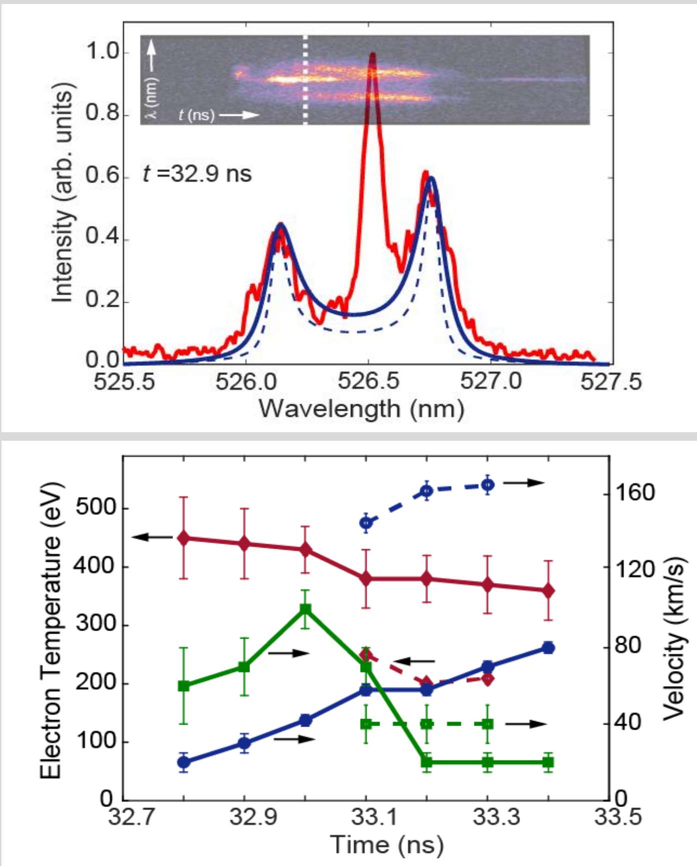

Top: Thomson scattering lineout with instrument function fit, 32 ns; bottom: Electron temperature (red), jet mean velocity (blue) and turbulent velocity (green).

- Electron temperature, bulk flow, and ion temperature/turbulent motion measurement in 50 μm³ region

- Typical electron temperature (for 5 ns drive)

$$T_e \sim 350 - 450\,\mathrm{eV}$$

- Ion temperature taken to be similar
  - Further broadening attributed to turbulent small-scale motions on scale of TS volume

$$u_l \sim 20 - 100\,\mathrm{km/s}$$

- Bulk motions (combined with large scale turbulent motions) found to have

$$u_0 \sim 20 - 80\,\mathrm{km/s}$$

X-ray emission

- Self-emission measured by X-ray framing camera, with pinhole resolution $l = 50\,\mu\mathrm{m}$
- Assuming an optically thin plasma, can relate relative emission intensity fluctuations to relative density fluctuations in interaction region (Churazov *et. al.*), and hence find latter power spectrum
- Results show power spectrum consistent with Kolmogorov scaling
  - In subsonic turbulence, typically expect spectrum of density and velocity fluctuations to have same scaling
- Conclusion: interaction region seems turbulent (or at least manifests stochastic motions)

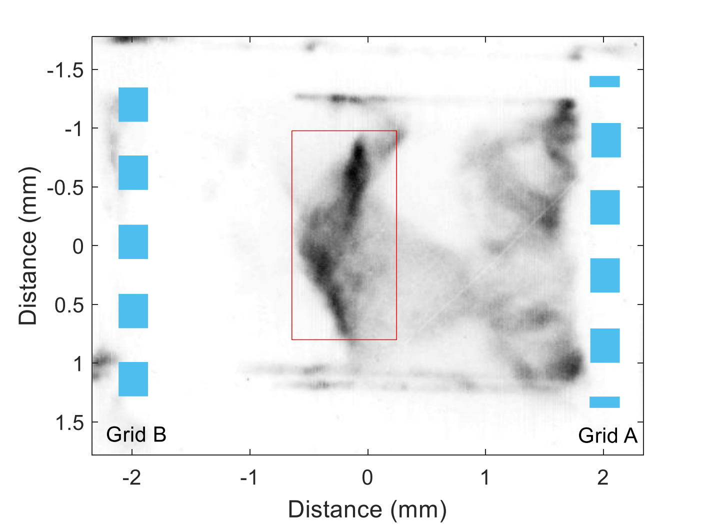

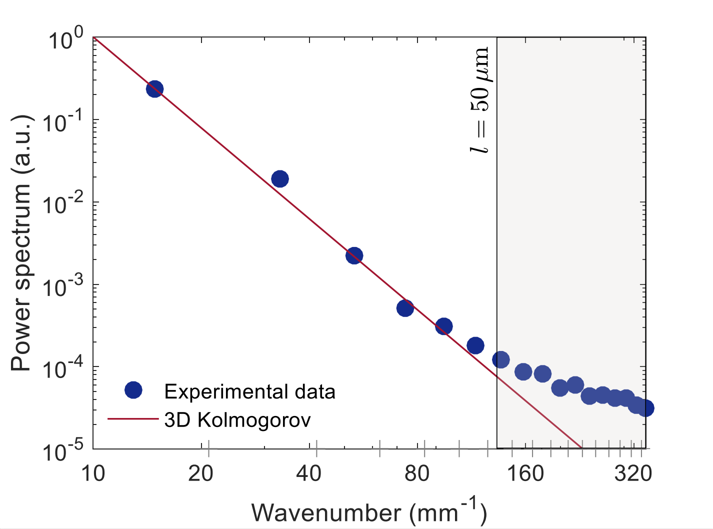

Proton radiography

- Proton beam (created by capsule implosion – two energies) used to image magnetic fields
- Early time radiographs show fields too weak to create large flux variations
- Later time show strong non-linear features (enhanced in 5 ns shots)

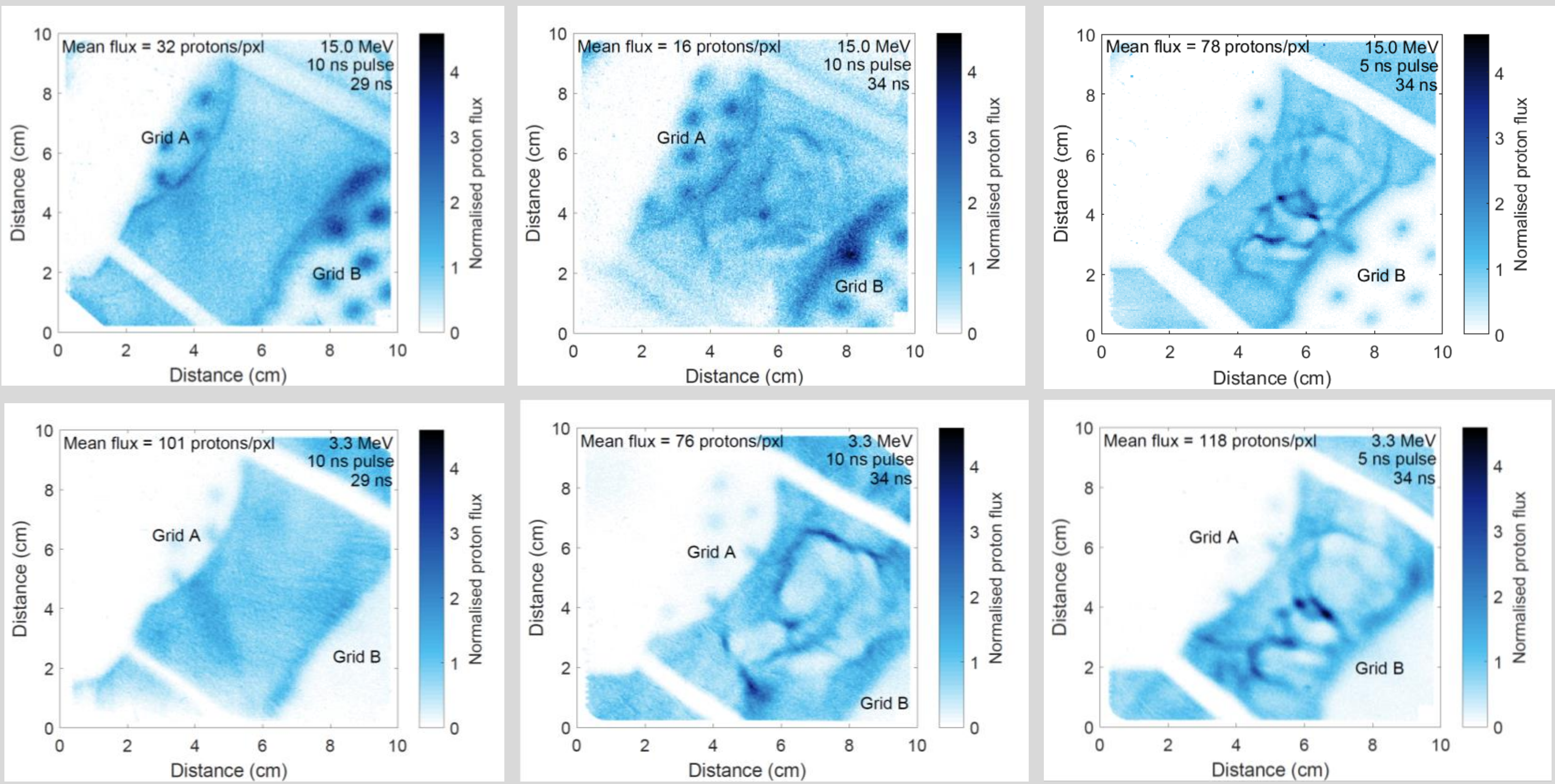

Polarimetry

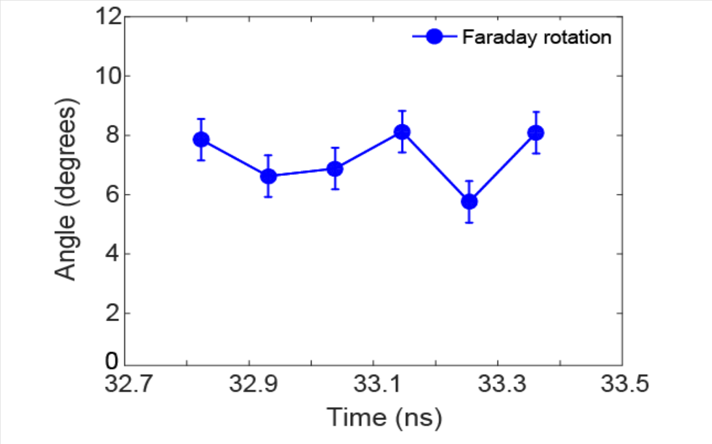

- Polarisation of Thomson scattering beam used to measure Faraday rotation effects
- Initial rotation taken from calibration shot
- Typical rotation found to be $\Delta\theta \sim 5^\circ - 10^\circ$
- For magnetic correlation scale l_B, rotation related to magnetic field strength by

$$B_{\|}(l_i \ell_B)^{1/2} \sim 17\,(\Delta\theta/7^\circ)(n_e/10^{20}\,\mathrm{cm}^{-3})^{-1}\,\mathrm{kG\,cm}$$

- Scaling dependence on l_B of proton flux magnitude has different scaling to polarimetry

$$\left\langle \mathbf{B}_\perp^2 \right\rangle^{1/2} \left(\frac{l_i}{l_B}\right)^{1/2} \sim 560 \left(\frac{\delta\Psi}{\Psi_0}\right) \mathrm{kG}$$

- This allows for self-consistent solution for $\left\langle \mathbf{B}^2 \right\rangle^{1/2}$ and l_B (assuming isotropy) to give

$$\left\langle \mathbf{B}^2 \right\rangle^{1/2} \sim 450 - 550\,\mathrm{kG} \qquad l_B \sim 0.06\mathrm{cm}$$

Flash simulations

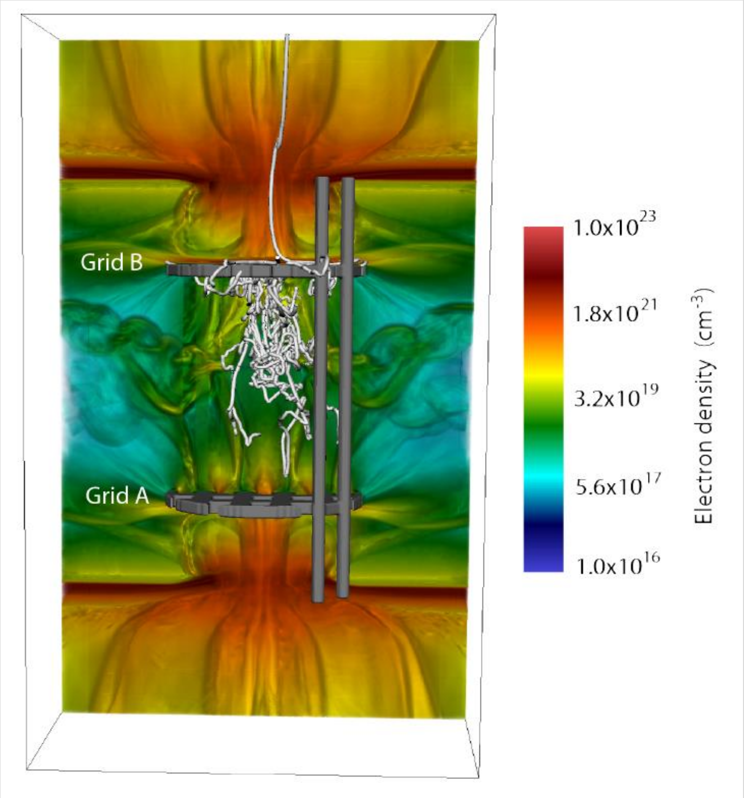

- Two-fluid laser-plasma simulation code used to complement experiment
  - Comparative diagnostic outputs generated
- Thomson scattering results for electron temperature and velocities from simulation and experiment consistent
  - Code predicts $T_e \approx T_i$ - justification for previous assumption
- Simulation used to give estimate of absolute density $n_e \sim 10^{20}\,\mathrm{cm}^{-3}$ (not measured experimentally)
- Initial (Biermann battery) seed fields found to have $\langle \mathbf{B}^2 \rangle^{1/2} \sim 25\,\mathrm{kG}$: shock compression and Biermann battery field generation in interaction region not sufficient to explain field growth

Plasma parameterisation

- Adopting experiment plasma parameters as

Input quantity	Value
M	6.5
Z	3.5
$T = T_e, T_i\,(\mathrm{eV})$	450
$n_e\,(\mathrm{cm}^{-3})$	10^{20}
$U, u_L\,(\mathrm{km/s})$	200
$L\,(\mathrm{cm})$	0.06
$B\,(\mathrm{G})$	$450,000$

we obtain estimates of theoretical plasma parameters shown opposite.

- Plasma is essentially well described as MHD, subsonic
- Prandtl number $\mathrm{Pr} \sim 1$, though sensitive to ion temperature assumption
- Ions seem un-magnetised, so resulting plasma closer to typical simulations than ICM

Quantity	Formula	Value
$\log\Lambda$	$23.5 - \log n_e^{1/2} T_e^{-5/4} - \sqrt{10^{-5} + \frac{(\log T_e - 2)^2}{16}}$	7
$\lambda_D\,(\mathrm{cm})$	$7.43\times10^{2}\,\frac{T^{1/2}}{(n_e(1+Z))^{1/2}}$	7.4×10^{-7}
Ma	u_L/c_s	1
β	$4.0\times10^{-11}\,\frac{nT}{B^2}$	12
$\lambda_e\,(\mathrm{cm})$	$2.04\times10^{13}\,\frac{T_e^2}{Z n_e \log\Lambda}$	1.7×10^{-3}
$\lambda_{ii}\,(\mathrm{cm})$	$2.88\times10^{13}\,\frac{T_i^2}{Z^4 n_i \log\Lambda}$	1.9×10^{-4}
$\tau_{ie}^{\epsilon}\,(\mathrm{s})$	$3.2\times10^{8}\,\frac{M T_e^{3/2}}{Z n_e \log\Lambda}$	8.0×10^{-9}
$\rho_e\,(\mathrm{cm})$	$3.37\,\frac{T_e^{1/2}}{B}$	1.4×10^{-4}
$\rho_i\,(\mathrm{cm})$	$1.44\times10^{2}\,\frac{M T_i^{1/2}}{ZB}$	4.9×10^{-3}
$\rho_e\lambda_e$	$6.05\times10^{12}\,\frac{B T_e^{3/2}}{Z n_e \log\Lambda}$	10
$\rho_i\lambda_{ii}$	$2.01\times10^{11}\,\frac{B T_i^{3/2}}{M^{1/2} Z^3 n_i \log\Lambda}$	0.039
$\nu\,(\mathrm{cm^2/s})$	$1.92\times10^{19}\,\frac{T_i^{3/2}}{M^{1/2} Z^4 n_i \log\Lambda}$	1.1×10^{3}
Re	$\frac{u_L L}{\nu}$	$\sim 1,100$
$l_\nu\,(\mathrm{cm})$	$\frac{L}{Re^{3/4}}$	3.1×10^{-4}
$\eta\,(\mathrm{cm^2/s})$	$2.4\times10^{5}\,\frac{Z\log\Lambda}{T_e^{3/2}}$	8.3×10^{2}
Rm	$\frac{u_L L}{\eta}$	$1,500$
Pr	$\frac{Rm}{Re}$	~ 1
$l_\eta\,(\mathrm{cm})$	$\frac{l_\nu}{Pr^{1/2}}$	3×10^{-4}

Conclusions and next steps

1. Platform seems to produce MHD-type, 'super-critical' Rm plasma undergoing stochastic motions

2. Significant field amplification (with stochastic structure) generated by interaction of jets
   - Dynamo mechanism likely candidate
   - Magnetic/kinetic field energy ratio approaching unity – $B^2/\mu_0 \rho u^2 \approx 0.1$

- Second round of experiments due next week
  - Pinhole set-up to be used as alternative (hopefully more quantitative) method for measuring particle deflections
  - Increase time-range of shots
  - New grid pattern to create larger, more symmetric interaction region

Proton radiography – improved analysis?

- Estimating magnetic fields correctly crucial to success of experiment – yet techniques described above qualitative.
  - Question: *can radiographs be analysed quantitatively?*

- Radiographic analysis often done by post-processing simulated EM fields
  - Good approach for simple configurations – but less effective for stochastic fields

- Example: FLASH magnetic fields generate radiographic image which seems quite different from actual radiograph

- Alternative approach: use asymptotic analysis to derive expression for flux in terms of magnetic field
  - 'Small/moderate' magnetic field *gradients* – RMS values and spectra extractable.
  - 'Large' gradients – spatial information lost, field strength statistics still accessible.

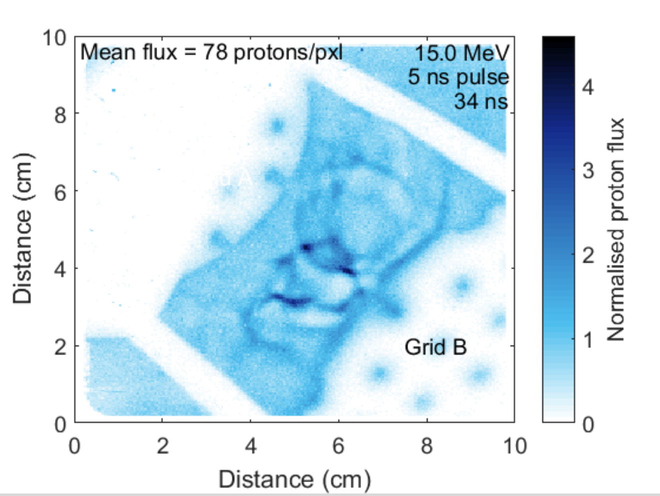

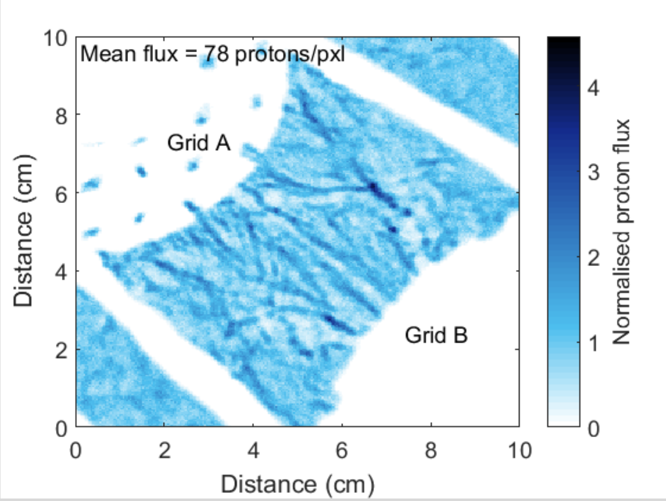

Diagnostic set-up

- Beam typically generated by TNSA (thermal spectrum of energies) or capsule implosion (two discrete energies)
- Usual set-up is done in paraxial limit

$$\delta\alpha \equiv \frac{l_i}{r_i} \ll 1$$

- Typical deflections $\delta\theta \ll 1$
- Fast speed of protons greatly simplifies physics governing beam
  - Self-interactions, kinetic instabilities, collisional effects (basically) negligible
- Electric forces smaller than magnetic forces

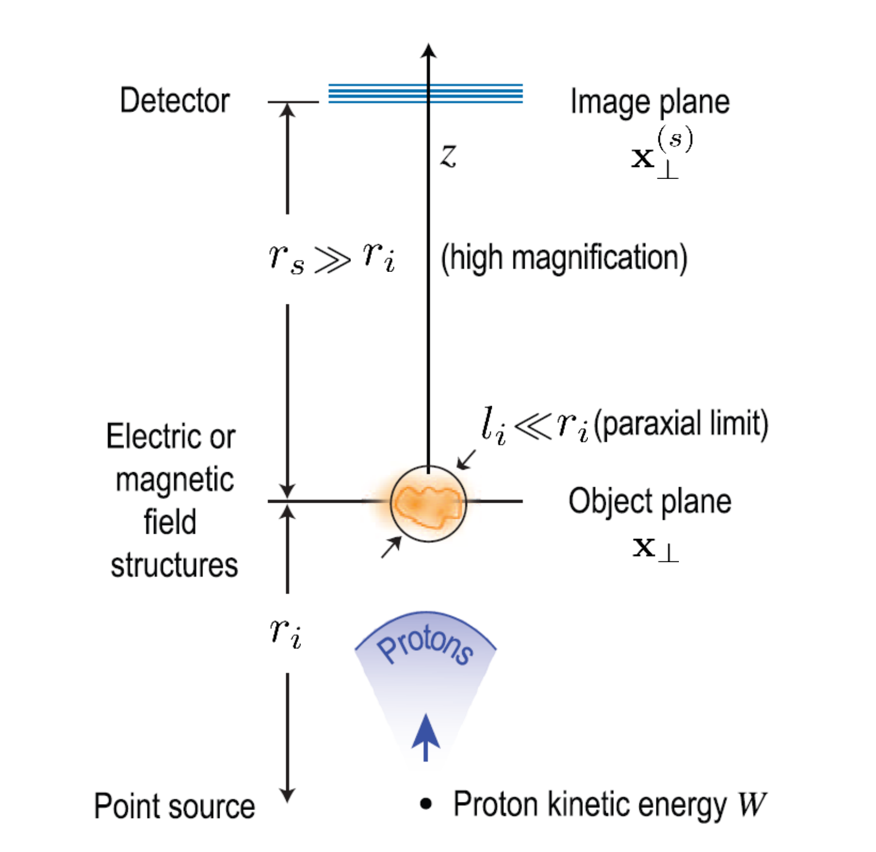

Kugland et. al. (2012)

Proton beam evolution equation

- Beam obeys governing Vlasov equation

$$\frac{\partial f}{\partial t} + \mathbf{v} \cdot \nabla f + \frac{e}{m_p c} \mathbf{v} \times \mathbf{B}(\mathbf{x}) \cdot \frac{\partial f}{\partial \mathbf{v}} = 0$$

- Exact solution

$$f(\mathbf{x}, \mathbf{v}, t) = \sum_{\mathbf{x}_0, \mathbf{v}_0} f_0(\mathbf{x}_0(\mathbf{x}, \mathbf{v}, t), \mathbf{v}_0(\mathbf{x}, \mathbf{v}, t)) \left| \frac{\partial(\mathbf{x}_0, \mathbf{v}_0)}{\partial(\mathbf{x}, \mathbf{v})} \right|$$

where characteristic ray mapping given by inverting particle trajectories

$$(\mathbf{x}(t), \mathbf{v}(t)) = \left(\mathbf{x}_0 + \int_0^t \mathbf{v}(t') \, \mathrm{d}t', \mathbf{v}_0 + \int_0^t \frac{e}{mc} \mathbf{v}(t') \times \mathbf{B}(\mathbf{x}(t')) \, \mathrm{d}t' \right)$$

- Since deflections $\delta\theta \ll 1$, try naïve asymptotic solution $\mathbf{v} = \mathbf{V} + \mathbf{w}$, with $\|\mathbf{w}\| \ll \|\mathbf{V}\|$

$$\mathbf{w}(t) = \frac{e}{m_p c} \mathbf{V} \times \int_0^t \mathbf{B}(\mathbf{x}(t')) \, \mathrm{d}t' \;\; [1 + \mathcal{O}(\delta\theta, \delta\alpha)]$$

- Generally helpful for simple fields (with some complications!); leads to scaling

$$\delta\theta \sim \frac{eBl_i}{m_p c V} \approx \frac{B(\mathrm{MG})}{2.6\,\mathrm{MG}} \quad \text{for DD 3.3 MeV protons, 1mm plasma}$$

Asymptotic approximations to deflection field

- Total deflection experienced by a particle with initial position $\mathbf{x}_{\perp 0}$ becomes

$$\mathbf{w}(\mathbf{x}_{\perp 0}) \equiv \mathbf{w}\left(\frac{l_i}{V}\right) = \frac{e}{m_p c V}\,\hat{\mathbf{z}} \times \int_0^{l_i} \mathbf{B}(\mathbf{x}(z')\,, z')\,\mathrm{d}z' \;\left[1 + \mathcal{O}(\delta\alpha, \delta\theta)\right]$$

- Deflection 'field' irrotational in sense that

$$\nabla_{\perp 0} \times \mathbf{w}(\mathbf{x}_{\perp 0}) = \mathcal{O}(\delta\alpha, \delta\theta)$$

and so can be written as the gradient of a potential

$$\mathbf{w}(\mathbf{x}_{\perp 0}) = \nabla\left(\frac{e}{m_p c V} \int_0^{l_i} \hat{\mathbf{z}} \cdot \mathbf{A}(\mathbf{x}(z')\,, z')\,\mathrm{d}z'\right) \;\left[1 + \mathcal{O}(\delta\alpha, \delta\theta)\right]$$

- Further asymptotic approximations possible – for example, expand around initial position

$$\mathbf{w}(\mathbf{x}_{\perp 0}) = \frac{e}{m_p c V}\,\hat{\mathbf{z}} \times \int_0^{l_i} \mathbf{B}(\mathbf{x}_{\perp 0}, z')\,\mathrm{d}z' \;\left[1 + \frac{l_i}{l_B}\mathcal{O}\left(\delta\alpha, \delta\theta, \frac{a}{r_i}\right)\right]$$

Propagation from plasma to imaging screen

- Beyond magnetic field configuration, particles undergo free-streaming: only real parts of phase space coordinates altered

- The magnetic fields induce a coordinate distortion to an initial regular grid carrying the flux distribution. If $r_s \gg l_i$, then in paraxial limit, perpendicular mapping satisfies

$$\mathbf{x}_\perp^{(s)} = \frac{r_i + r_s}{r_i}\mathbf{x}_\perp + r_s \frac{\mathbf{w}(\mathbf{x}_\perp)}{V} + \mathcal{O}\left(\frac{l_i}{r_s}\right)$$

- For a distribution function arising from a point source, the flux becomes

$$\Psi\left(\mathbf{x}_\perp^{(s)}\right) = \sum_{\mathbf{x}_\perp^{(s)}=\mathbf{x}_\perp^{(s)}(\mathbf{x}_{\perp 0})} \frac{\left(\frac{r_i}{r_s+r_i}\right)^2 \Psi_{\perp 0}\left(\mathbf{x}_{\perp 0}\left(\mathbf{x}_\perp^{(s)}, \frac{r_s}{V}\right)\right)}{\left|1 + \frac{r_s r_i}{(r_s+r_i)V}\nabla_{\perp 0} \cdot \mathbf{w}(\mathbf{x}_{\perp 0}) + \left(\frac{r_s r_i}{(r_s+r_i)V}\right)^2 \det \frac{\partial \mathbf{w}(\mathbf{x}_{\perp 0})}{\partial \mathbf{x}_{\perp 0}}\right|}$$

Numerical example

- Test theory by comparing results of test particles numerically propagated through field configuration, field strength $\left\langle \mathbf{B}^2 \right\rangle^{1/2} = 5\,\mathrm{kG}$

- Good qualitative (and quantitative) agreement

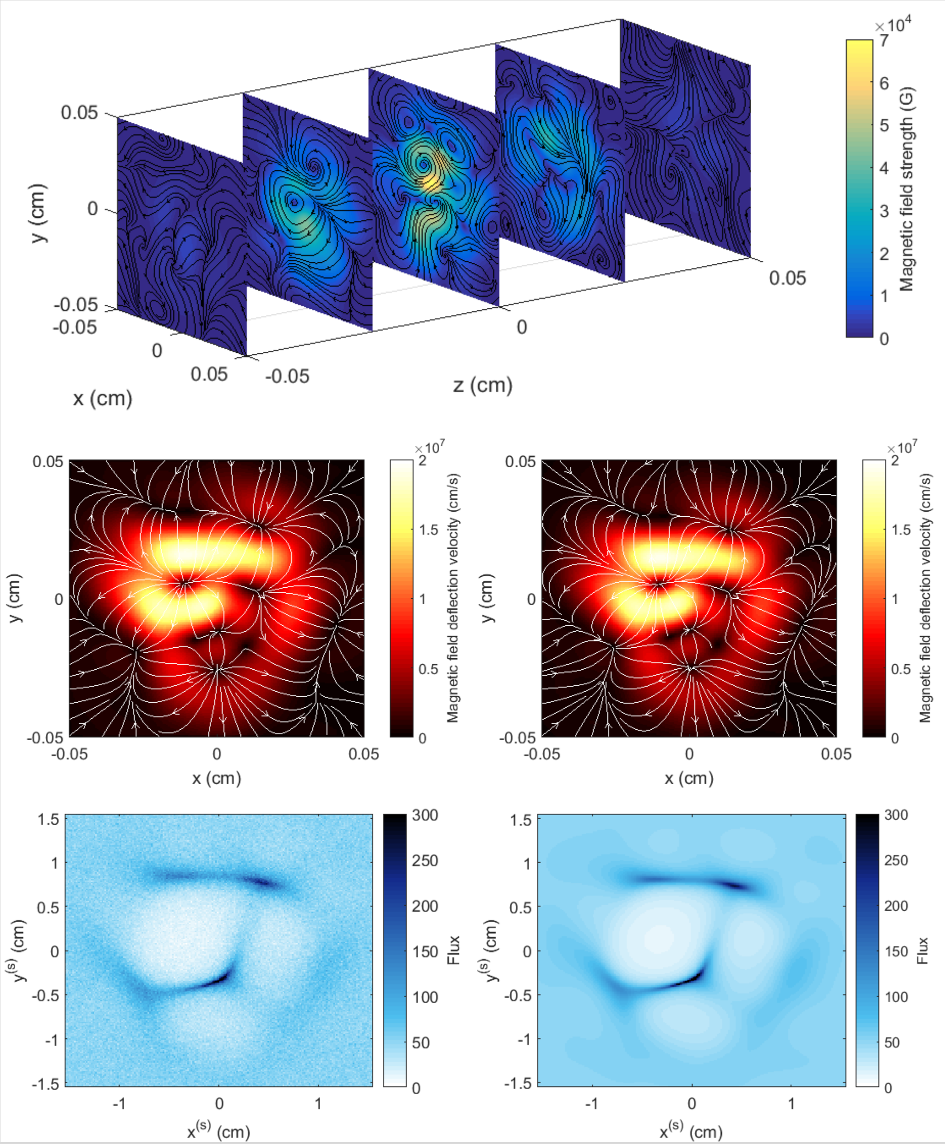

UNIVERSITY OF OXFORD

Smearing

- By choosing a different initial distribution function, the effects of smearing can be included in kinetic model.

- Smeared flux related to point-source flux by

$$\tilde{\Psi}\left(\mathbf{x}_{\perp}^{(s)}\right) = \int \mathrm{d}^2\tilde{\mathbf{x}}_{\perp}^{(s)}\, \Psi\left(\tilde{\mathbf{x}}_{\perp}^{(s)}\right) S\left(\mathbf{x}_{\perp}^{(s)} - \tilde{\mathbf{x}}_{\perp}^{(s)}\right)$$

where the point spread function

$$S\left(\mathbf{x}_{\perp}^{(s)} - \tilde{\mathbf{x}}_{\perp}^{(s)}\right) = P\left(\frac{\tilde{\mathbf{x}}_{\perp}^{(s)} - \mathbf{x}_{\perp}^{(s)}}{r_s} V\right)$$

is related to the initial spread in perpendicular velocities

- Again well matched by numerical experiments.

- If smearing effect small, original image recoverable with deconvolution algorithm – though such analysis prone to instabilities

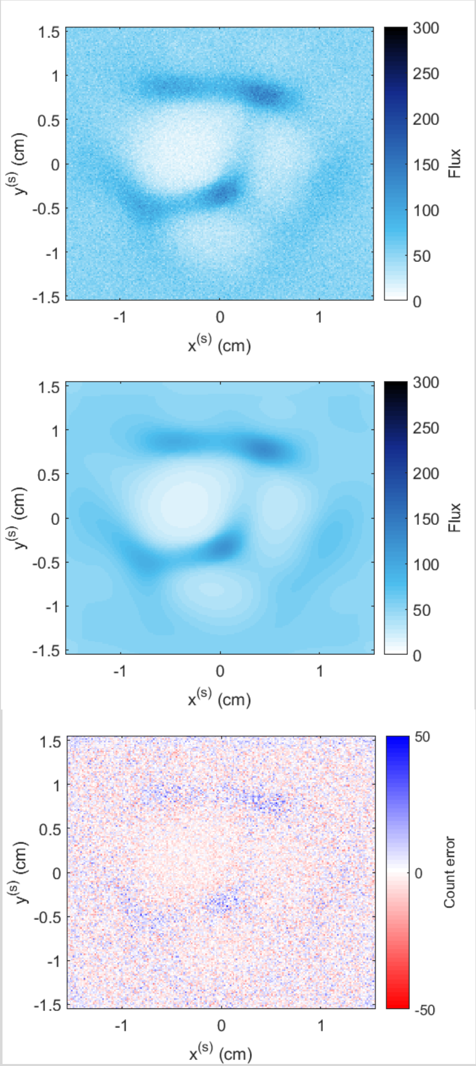

Physical interpretation of radiographic images

- Meaning of flux map dependent on *contrast parameter*

$$\mu \equiv \frac{\delta\theta}{\delta\alpha}\frac{r_s}{r_s + r_i}\frac{l_i}{l_B} = \frac{r_s\,\delta\theta}{\tilde{l}_B}$$

for $\tilde{l}_B$ the stochastic field correlation scale.

$\underline{\mu \ll 1}$ - 'linear regime', where relative flux is proportional to the path-integrated z-component of current:

$$\frac{\delta\Psi\left(\mathbf{x}_\perp^{(s)}\right)}{\Psi_0^{(s)}\left(\mathbf{x}_\perp^{(s)}\right)} = \frac{r_s r_i}{r_s + r_i}\frac{4\pi e}{m_p c^2 V}\int_0^{l_i} j_z\left(\mathbf{x}_{\perp 0}\left(1 + \frac{z'}{r_i}\right), z'\right)\mathrm{d}z'$$

$\underline{\mu \leq \mu_{crit}}$ - 'non-linear injective regime' – coordinate distortions, but no multi-valuedness

$\underline{\mu > \mu_{crit}}$ - 'multivalued regime' – coordinate distortions dominate flux morphology

$\underline{\mu \gg 1}$ - 'high contrast': spatial information about structure size lost, image displays PDF of deflection field

Numerical example

- Flux generated from stochastic Gaussian field with Kolmogorov power law for various contrasts

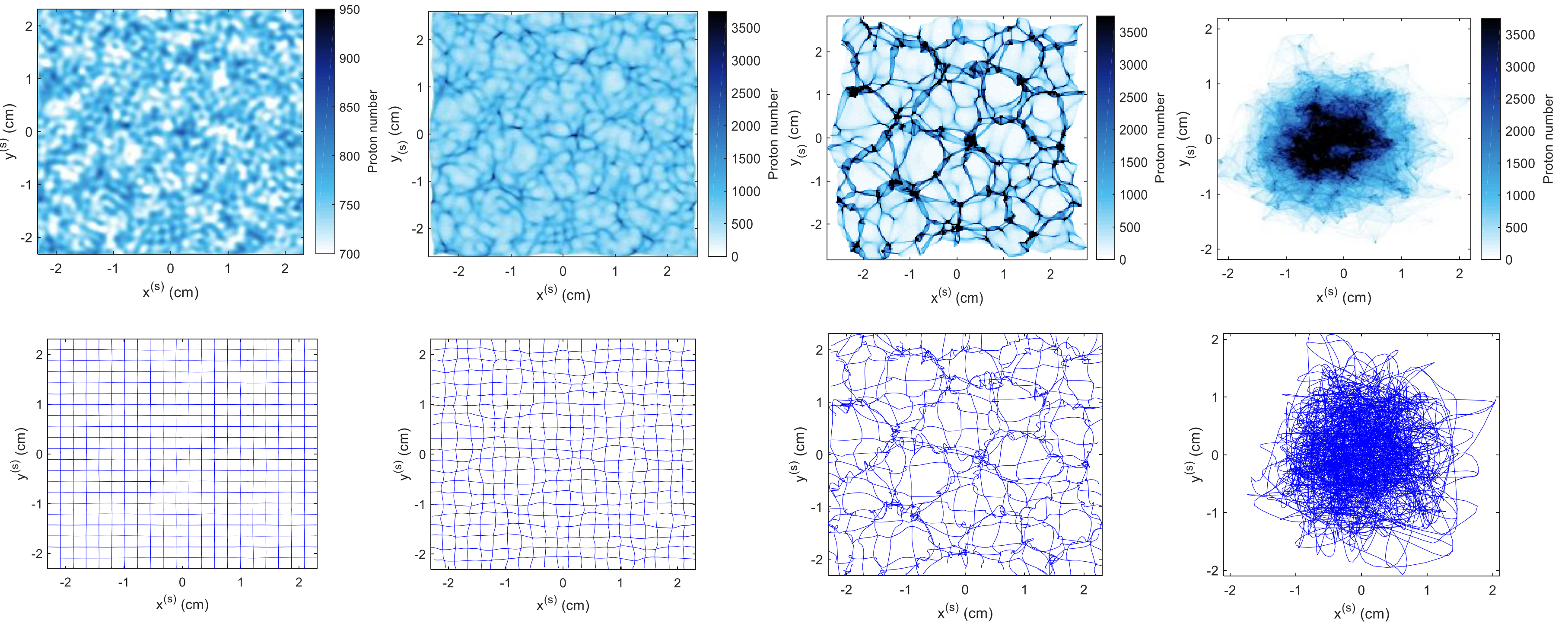

$$\left\langle \mathbf{B}^2 \right\rangle^{1/2} = 2\,\mathrm{kG} \quad r_i = 1\,\mathrm{cm} \quad \mu = 0.2$$

$$\left\langle \mathbf{B}^2 \right\rangle^{1/2} = 20\,\mathrm{kG} \quad r_i = 1\,\mathrm{cm} \quad \mu = 2$$

$$\left\langle \mathbf{B}^2 \right\rangle^{1/2} = 125\,\mathrm{kG} \quad r_i = 1\,\mathrm{cm} \quad \mu = 10$$

$$\left\langle \mathbf{B}^2 \right\rangle^{1/2} = 500\,\mathrm{kG} \quad r_i = 100\,\mathrm{cm} \quad \mu = 5,000$$

UNIVERSITY OF OXFORD

Stochastic fields – theoretical background

- Heuristically, expect particle undergoing motion through fields to experience a velocity deflection accumulating as a random walk (provided small angle deflections)

$$\delta w \sim \frac{e\left\langle \mathbf{B}^2 \right\rangle^{1/2}}{m_p c}\sqrt{l_i l_B} \qquad \delta\theta_{RW} \sim \frac{w}{V} \sim \frac{e\left\langle \mathbf{B}^2 \right\rangle^{1/2}}{m_p c V}\sqrt{l_i l_B} \sim \delta\theta_C \sqrt{\frac{l_B}{l_i}}$$

- The contrast then scales as

$$\mu_{RW} \sim \frac{\delta\theta_{RW}}{\delta\alpha}\frac{r_s}{r_s + r_i}\frac{l_i}{l_B} \sim \frac{r_s}{r_s + r_i}\frac{e\left\langle \mathbf{B}^2 \right\rangle^{1/2} r_i}{m_p c V}\sqrt{\frac{l_i}{l_B}} \sim \mu_C \sqrt{\frac{l_i}{l_B}}$$

- Thus for a fixed field strength, as the correlation scale of a field decreases the typical deflection size is reduced, but contrasts increase.
  - At very small scales, local flux behaviour determined by deflection magnitude – well modelled by a diffusive picture (see later).

- Scalings supported by analytical correlation analysis, and numerical simulations.

Spectral reconstruction

- In the linear regime, the spectra of the deflection field and the flux respectively can be linked to that of magnetic fields:

$$E_B(k) = \frac{m_p^2 c^2}{2\pi l_i e^2} k^2 \hat{C}(k)$$
$$= \frac{1}{2\pi} \frac{m_p^2 c^2 V^2}{e^2 r_s^2 l_i} \hat{\eta}\left(\frac{r_i}{r_s + r_i} k\right)$$

- Numerical tests on field with power law spectrum (index -2), and field strength $\langle \mathbf{B}^2 \rangle^{1/2} = 0.5\,\mathrm{kG}$, demonstrate feasibility of method.

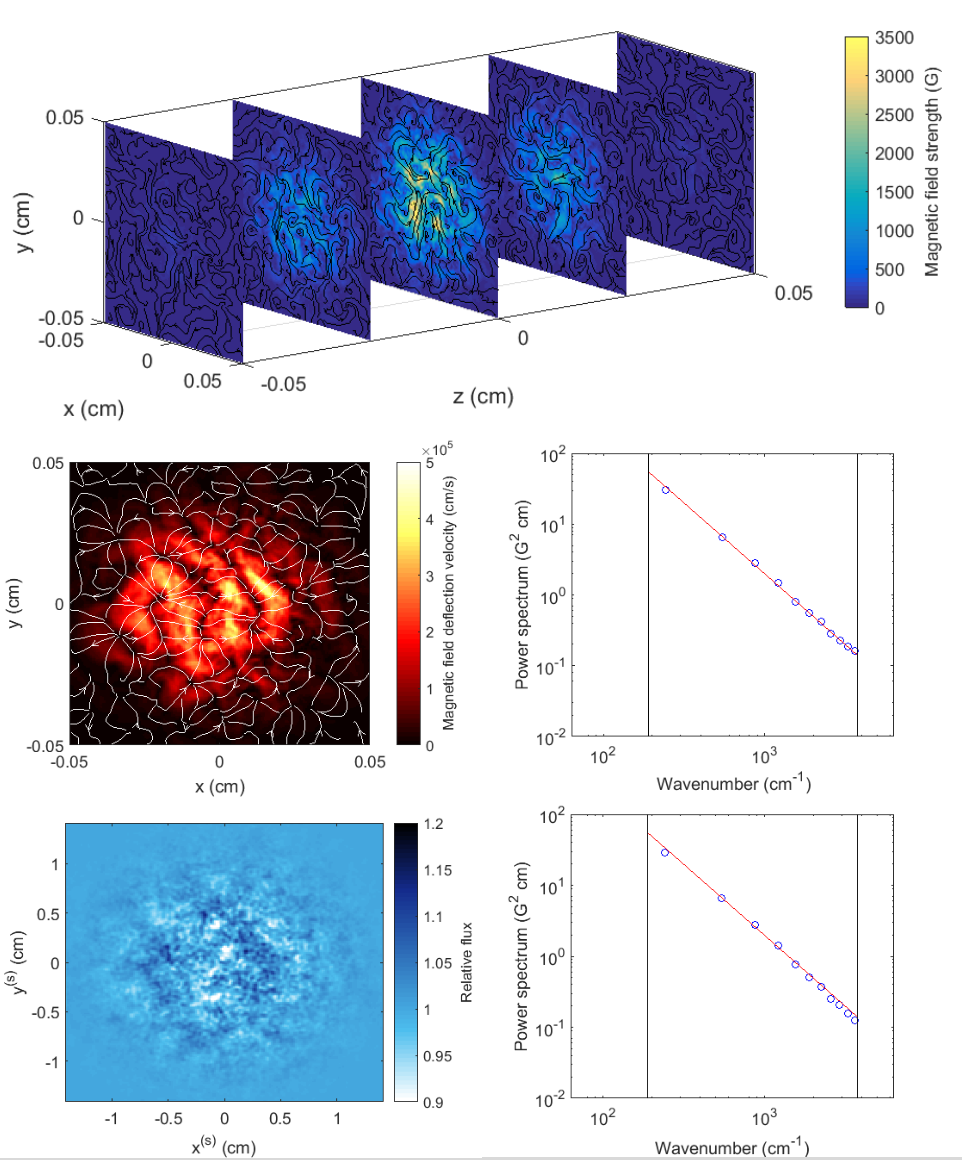

Spectral reconstruction and non-linear effects

- Problem: for highest contrasts, optical distortion of flux affects spectral shape.
- Deflection field is (asymptotically) linear in the magnetic field, so is not affected by this.
- Q: can the deflection field be recovered from the flux image ('reconstruction')
  - A: *yes* – but only if the coordinate mapping is injective
- Monge-Ampère equation (opposite) has unique convex solution with Neumann BCs.

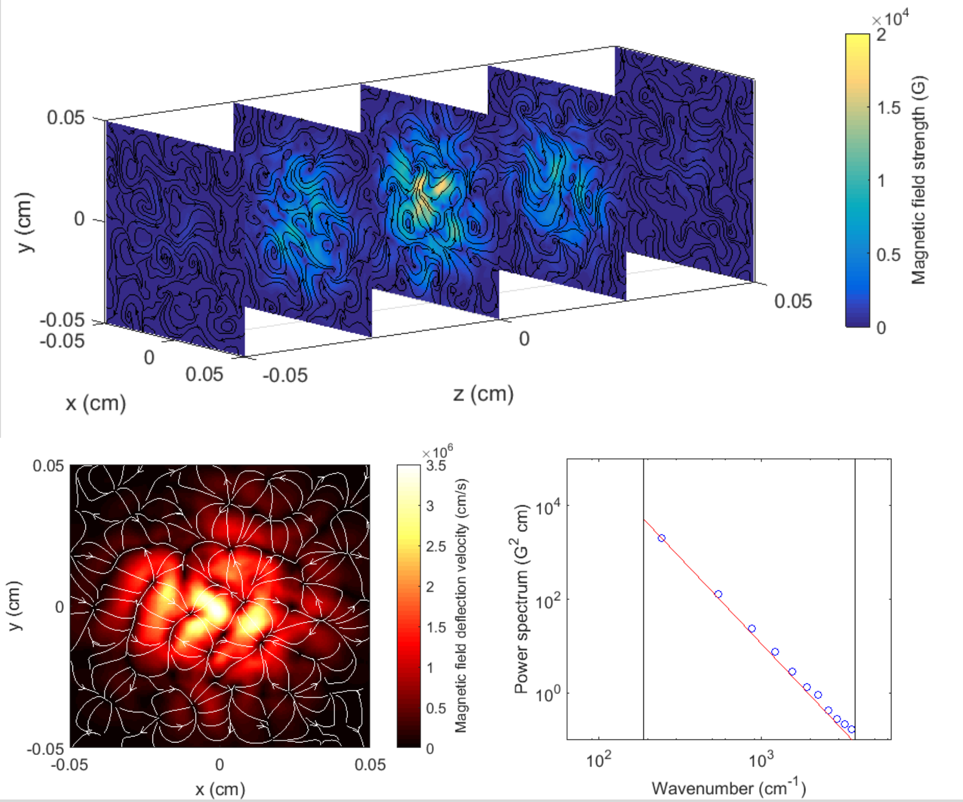

$$\det \nabla\nabla\phi(\mathbf{x}_{\perp 0}) = \frac{\Psi_{\perp 0}(\mathbf{x}_{\perp 0})}{\Psi(\nabla\phi(\mathbf{x}_{\perp 0}))}$$

UNIVERSITY OF OXFORD

Non-linear flux spectral distortion

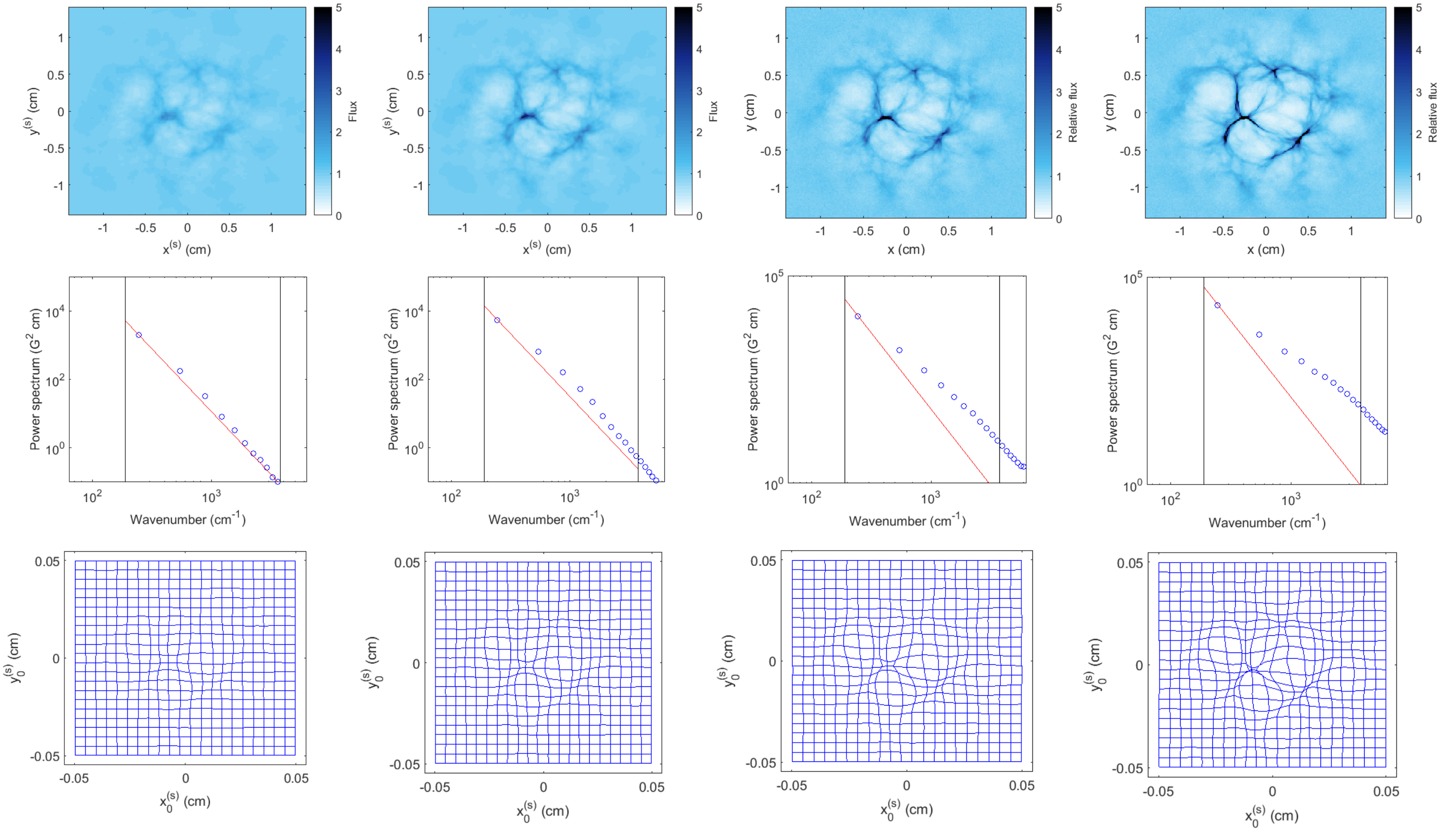

Non-linear reconstruction

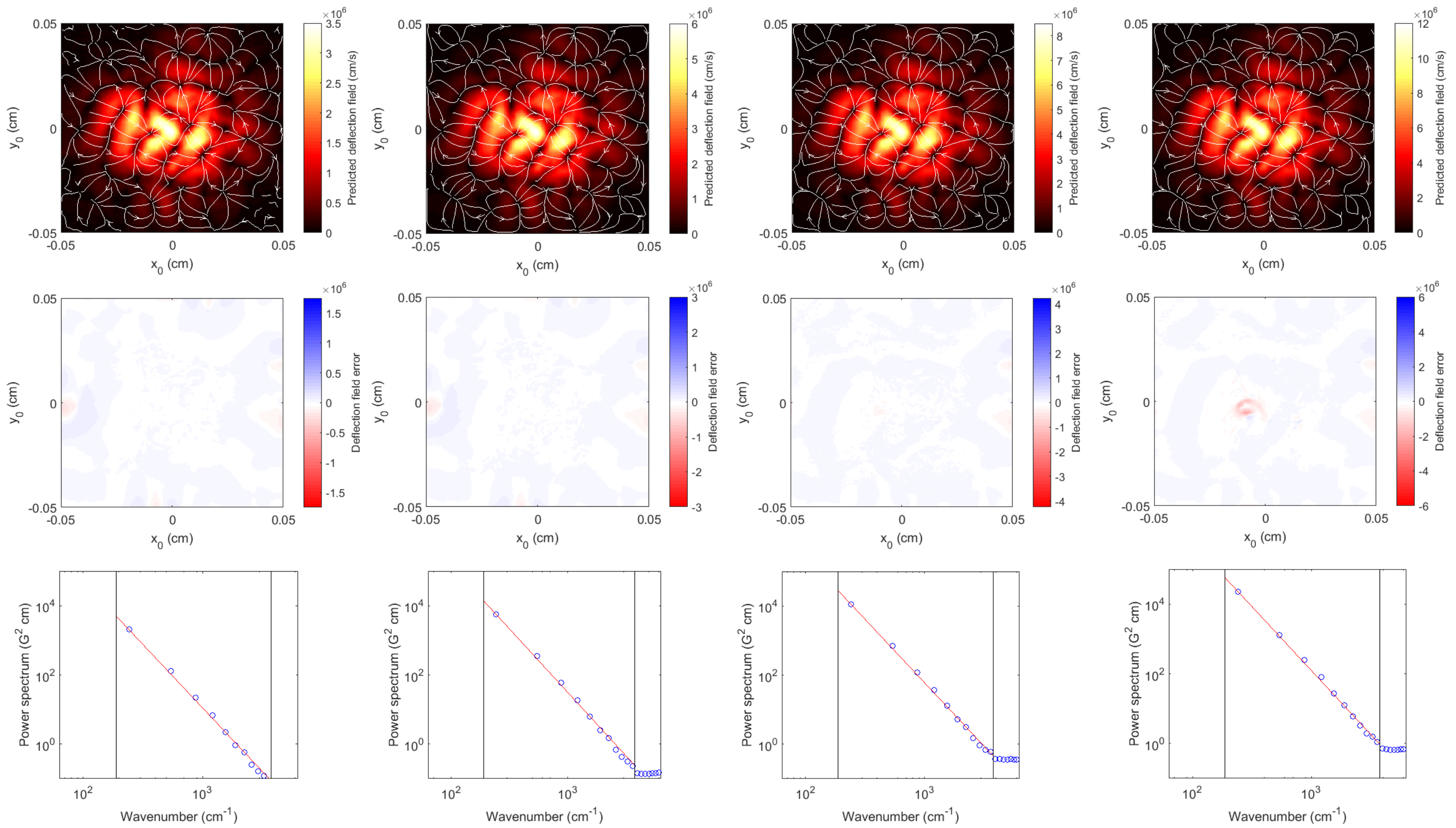

UNIVERSITY OF OXFORD

Non-linear reconstruction on multi-valued images

- If an image has multi-valued flux regions, the algorithm will behave as if the flux is single-valued, so the solution will be invalid.
- Can be shown analytically (Gangbo *et. al.*) that solution of Monge-Ampere equation is always a lower bound on the deflection field RMS (as illustrated numerically).

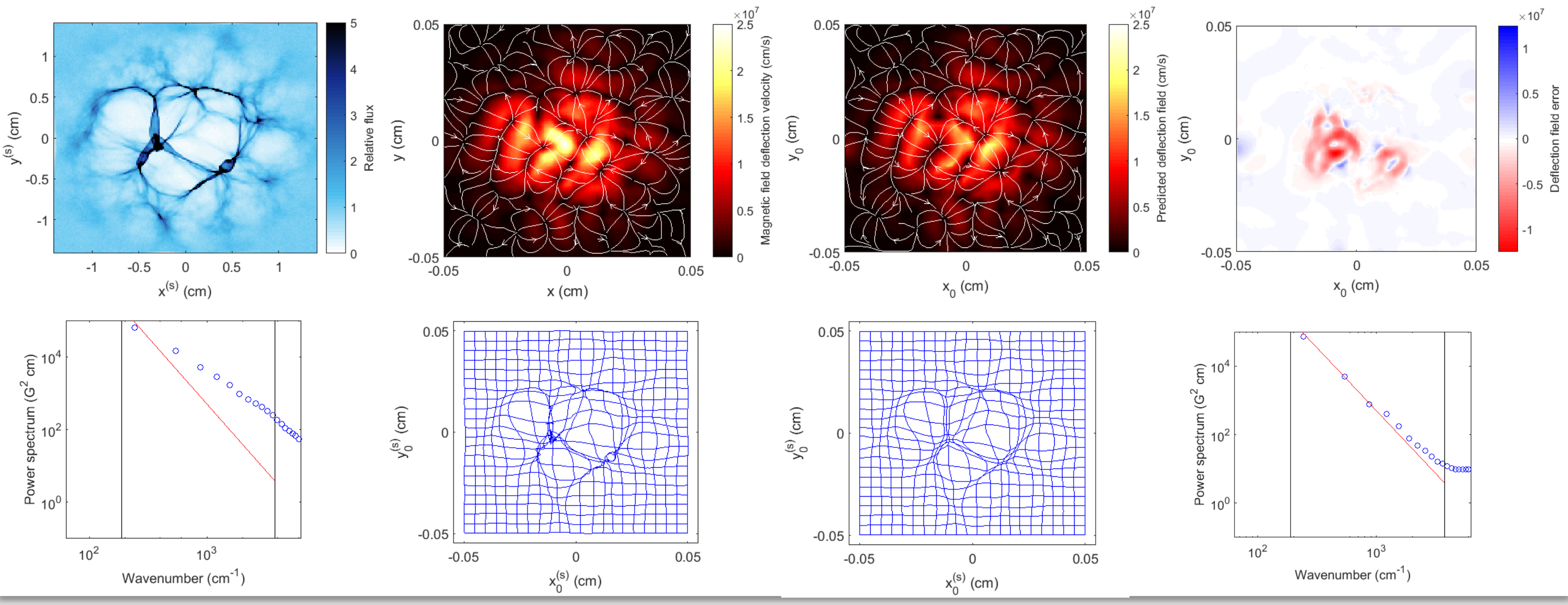

Small-scale fields – diffusive picture

- There has been extensive work done modelling the evolution of a beam of particles through stochastic magnetic fields diffusively.
  - Bykov and Toptigin (1966) derive a governing equation for the ensemble averaged distribution function of non-interacting, unmagnetised test particles using quasi-linear theory
  - The result of such an attempt is typically a diffusion tensor, the form of which being dependent on both properties of the beam and the field.

- For homogenous, isotropic stochastic magnetic fields satisfying $l_B \ll l_i$ (and using a typical beam), can deduce diffusion equation using QL theory on Vlasov equation (assuming no collective effects) for particle distribution $\langle f \rangle$ (ensemble averaged)

$$\frac{\partial \langle f \rangle}{\partial t} + \mathbf{w} \cdot \tilde{\nabla} \langle f \rangle = D_w \frac{\partial}{\partial \mathbf{w}_\perp} \cdot \frac{\partial \langle f \rangle}{\partial \mathbf{w}_\perp}$$

for diffusion coefficient and typical diffusion velocity

$$D_w = \frac{V e^2 \left\langle \mathbf{B}^2 \right\rangle l_B}{3 m^2 c^2} \qquad \Delta w = \frac{2}{\sqrt{3}} \frac{e \left\langle \mathbf{B}^2 \right\rangle^{1/2}}{mc} \sqrt{l_i l_B}$$

Summary and next steps

1. Physical interpretation of proton images arising from magnetic fields depends on contrast parameter μ
   - Small μ - flux variations describe current fluctuations
   - Moderate μ - non-linear coordinate distortion.
   - Large μ - probability density function of field strengths.
2. Decreasing correlation length of stochastic field decreases deflections, increases contrasts
   - Shift from regime in which spatial statistics of fields reflected in flux/deflections into diffusive picture.
3. For small to moderate μ, spectrum and mean field strengths extractable.
   - Use of reconstruction techniques avoids non-linear distortion.

- Still work in progress: application to actual radiographs
  - Reconstruction method non-local, so sensitive to boundary conditions